Perspective

Electron tomography: a tool for 3D structural probing of heterogeneous catalysts at the nanometer scale

Transmission electron microscopy delivers a versatile range of techniques for the structural characterization of inorganic solids. For recent reviews we refer to [1,2]. An exciting new tool commercially available for three-dimensional structural investigations using transmission electron microscopy (3D-TEM) is electron tomography. The method enables the characterization of structures hundreds of nanometers in size at nanometer-scale resolution. Conceptually related to other tomographic technique like X-ray microtomography, computer tomography, magnetic resonance imaging or positron emission tomography, as used in materials science or medical applications, it enables the *non-destructive* investigation of the *interior* of truly *unique* structures. However, making use of transmission electron microscopy images, the resolution of electron tomography is in the nanometer range and thus in between that of atom probe tomography (atomic) and X-ray microtomography (μm). Possible applications for heterogeneous catalysis (both for academic and industry settings) include the determination of the 3D shape, volume, connectivity and location of meso- and macropores inside a support material. Moreover, size and location of metal particles inside the material can be visualized unambiguously and subjected to statistical evaluation (Fig. 1). The unique possibilities of electron tomography can readily be understood from the two basic steps that the method is based on (1) acquisition of *projection* images of the structure under investigation under different tilt angles (tilt series) and (2) calculation of the *3D reconstruction/tomogram* (interior densities) of the sample volume from these projections, typically via *weighted backprojection* or related methods.

A strong advantage of electron tomography is that it does not depend on averaging over unit cells or particles. The method enables the investigation of truly unique structures and is thus capable to visualize internal inhomogenities of samples (e.g. distribution of metal particles in catalysts [3–5]) in three dimensions. In addition, it can complement macroscopic methods like nitrogen physisorption to elucidate the relationship between microscopic structure and bulk characteristics (between form and function) of heterogeneous catalysts [6–8]. Since the method does not include averaging over unit cells or particles, the resolution will rather be in the nanometer than the atomic range (as possible with, e.g. electron diffraction/crystallography), as it is finally determined by the level of signal to noise in the projection images (tilt series).

Electron tomography data acquisition can also be regarded as a kind of super-stereology (for an application of stereology to zeolite mesopore structure determination, see e.g. [9]). Instead of images taken at only two different tilt angles, a tomographic data set might consist of more than 151 images taken over an angular range of 150°. Basically speaking, the more images and the larger the angular range, the higher the resolution will be within a 3D reconstruction. A rule-of-thumb for the achievable resolution equals three times the thickness of the sample divided by the number of images. Thus for a 100 nm thick sample the resolution would correspond to 2 nm for the 151 images. However, with certain electron microscopy acquisition modes, which necessitate high electron doses (e.g. energy filtered imaging) or electron beam sensitive samples (e.g. MCM-41), it might be necessary to reduce the number of exposures to trade in resolution for structural preservation. It should be noted, however, that the *practical* achievable resolution seems to be rather better than worse than the calculated value. Determination of the location of 1 nm sized metal particles inside a less dense matrix was shown for tomograms gained from high angular annular dark-field [10–12] and bright-field transmission electron microscopy images [13].

A prerequisite for the calculation of 3D reconstructions from electron micrographs in electron tomography is that the registered image contrast must be a projection of some physical characteristic of the sample, e.g. its mass/electron density. This implies that besides conventional bright-field transmission electron microscopy, dominated by phase and/or scattering contrast, several different modes of image
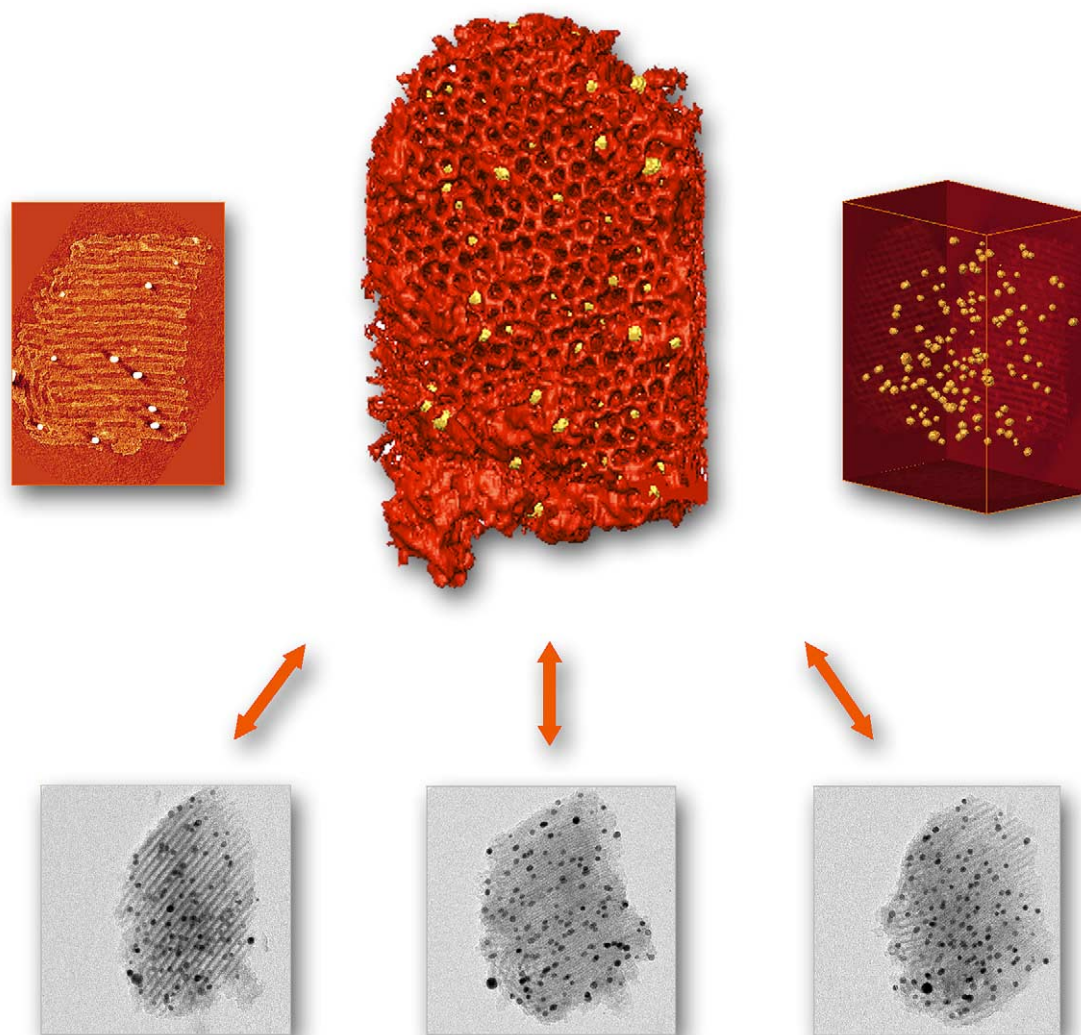
Fig. 1. The center panel of the top three images shows the surface rendered visualization of the reconstructed density of an Au/SBA-15 model catalyst particle ($\sim 256\,\mathrm{nm} \times 256\,\mathrm{nm} \times 166\,\mathrm{nm}$). 3D reconstructions like these can be utilized to determine the 3D shape, volume, connectivity and location of pores inside a support material. Moreover, the size and location of Au particles inside the material can be seen unambiguously (left: virtual cross-section—thickness 0.64 nm—through the reconstruction, right: surface rendering of gold particles—size 8 nm) and subjected to statistical evaluation. This kind of information could not be gained from a single transmission electron micrograph only (due to overlap of structures in projection). The slices at the bottom display three of the 151 electron microscopy projection images ($-55°$, $0°$ and $+55°$ tilt angle) that were used to calculate the volume. The two-sided arrows indicate the reversible process of projection and backprojection.

acquisition can be utilized in electron tomography to give insight into different characteristics of the sample. Energy filtered transmission electron microscopy (EFTEM) and X-ray spectroscopic imaging, for instance, enable the mapping of local concentrations of selected chemical elements. Certain other acquisition modes, on the other hand, are unsuitable (e.g. images based on Bragg angle diffraction contrast). In this case, however, the problem can be overcome by acquiring projection images with high angular annular dark-field/Z-contrast scanning transmission electron microscopy (HAADF-STEM).

The potential of electron tomography in the determination of the location of metal particles inside a supporting material has been demonstrated in a series of inspiring experiments. First-of-its-kind results on the unequivocal determination of the location of silver particles with a diameter of 10–40 nm in the interior or on the surface of a supporting material were obtained with Y zeolites (NaY) [3,4]. Also in experiments with SBA-15 model catalysts, which were either loaded with gold or contained 2–3 nm zirconia particles, unequivocal information on the location of these particles inside the support was obtained and the non-uniform distribution of particles over the mesopores explained the two-step desorption isotherm in nitrogen physisorption measurements [5]. Exciting results regarding the alumina distribution and thus an indication for the generation process of mesopores in zeolites were obtained by the comparison of reconstructions from steamed zeolite Y

Table 1
Development of electron tomography

				2001: routine application of TEM tomography in catalysis by Janssen/de Jong/Koster [6,7].
	1960's: first applications of tomography related technique in electron microscopy in biological sciences (*1982 Nobel Prize for Klug*)	1990's: routine application of TEM tomography in biological sciences	2000: first application of TEM tomography in catalysis by Geus/Janssen/de Jong/Koster [3,4]	2001: first applications of electron tomography to HAADF-STEM and spectroscopic (EFTEM, EDX) images by Midgley/Weyland [14] and Möbus [15]
Timeline				
1917: formulation of mathematical base for tomographic techniques by Radon (*Radon Transform*)	1960's: development of X-ray computerized tomography (*1979 Noble Prize for Cormack and Haunsfield*)	1990's: development of automated TEM tomography by Agard [18] and Baumeister [19] 1990: first commercial systems enable data acquisition in ~4 h		2001: development of pre-calibration electron tomography by Koster/Ziese [20,21] 2001: commercial systems making use of pre-calibration enable improved accuracy and data acquisition in ~30–60 min

The timeline focuses on the development and availability of the instrumentation for electron tomography and the application of the technique in heterogeneous catalysis. For the sake of clarity, several major steps, which took place throughout the 1960–1980s and that are the base of modern automated electron tomography, like e.g. the thorough evaluation of the underlying theory as well as the development of CCD cameras for fast image acquisition, are not taken into account.

(USY) and steamed and acid-leached zeolite Y (XVUSY) [6–8]. While the external surface as well as the walls of the mesopores in USY were covered with a darker layer, which is supposed to be amorphous alumina that was deposited during steaming, no such features were observed and thus were probably removed in the acid-leached XVUSY. All measurements were backed by results gained from nitrogen physisorption and XPS. The first application of electron tomography that utilizes high angular annular dark-field imaging to overcome the limitation of diffraction contrast, which disables the use of conventional bright-field transmission electron microscopy for certain materials, were conducted with Pd_6Ru_6 particles supported on MCM-41 [10,11]. Both, the 3D structure of the 3 nm wide pores and the distribution of the 1 nm sized Pd–Ru particles inside them, could be shown with great clarity. At the same time, important first experiments in the direction of spectroscopic tomography were made. Inclusions of chromium rich carbide structures in a 316 stainless steel and of Y_2O_3 nanoparticles in a polycrystalline FeAl intermetallic alloy were characterized by 3D mapping of the chromium and iron distributions, respectively, by energy filtered electron tomography [14,15].

What makes bright-field electron tomography a powerful tool instead of just a method with great potential for 3D characterization of samples at the nanometer-resolution range is its commercial availability. While material science is quite a newcomer in the field of electron tomography, the method has matured and become established in the biological sciences over the last two decades (for reviews, see e.g.

[16,17]). Automation efforts [18–21] led to a situation where in the meantime commercial systems are available that enable data acquisition for bright-field transmission electron microscopy tomography in between half and 1 h (correlated to demands in accuracy—with current hardware and software), whereas manual data acquisition would require several hours (Table 1). The authors were also impressed by the performance of a software prototype for the automated acquisition of Z-contrast tilt series that was recently made available for usage to them by FEI Co. (Eindhoven, The Netherlands).

The instrumental setup for electron tomography is based on a transmission electron microscope, equipped with a slow-scan CCD camera for image acquisition and a high-tilt sample stage and holder. The efficient usage of the method (acquisition of ~150 images) necessitates employing specialized software for remote control of microscope (e.g. tilting, relocation and focusing of samples) and camera. Certain applications will necessitate the use of electron microscopes with specialized equipment like field emission guns, higher electron voltages, high angular annular dark-field detectors, electron energy loss spectrometers or large area CCD cameras. However, we have found that a moderate setup with a 200 kV electron microscope equipped with a LaB_6 filament (Tecnai20, FEI) and a CCD camera run in a 1K × 1K mode (TemCam, TVIPS, Gauting, Germany) has enabled us to successfully investigate meso- and macropores, as well as the distribution of nanometer-sized metal particles inside several amorphous (alumina) silica(te) catalyst systems [3–8] (Fig. 1).

Future applications of electron tomography in catalysis will emphasize on spectroscopic imaging for the 3D mapping of local concentrations of selected chemical elements. In situ measurements of the active catalyst, however, do not seem to be feasible for the time coming, because of the discrepancy between the time scale on which reactions take place and the time required for data acquisition.

For other aspects on the application of electron tomography to material sciences samples, we would like to draw the attention to the reviews of de Jong and Koster [22], Midgley and Weyland [23] and Möbus et al. [24].

Acknowledgements

References

[1] A.K. Datye, J. Catal. 216 (2003) 144–154.
[2] J.M. Thomas, O. Terasaki, Top. Catal. 21 (4) (2002) 155–159.
[3] A.J. Koster, U. Ziese, A.J. Verkleij, A.H. Janssen, K.P. de Jong, J. Phys. Chem. B 104 (2000) 9368–9370.
[4] A.J. Koster, U. Ziese, A.J. Verkleij, A.H. Janssen, J. de Graaf, J.W. Geus, K.P. de Jong, Stud. Surf. Sci. Catal. 130 (2000) 329–334.
[5] A.H. Janssen, C.-M. Yang, Y. Wang, F. Schüth, A.J. Koster, K.P. de Jong, J. Phys. Chem. B. 107 (2003) 10552–10556.
[6] A.H. Janssen, A.J. Koster, K.P. de Jong, Stud. Surf. Sci. Catal. 135 (2001) 2144–2151.
[7] A.H. Janssen, A.J. Koster, K.P. de Jong, Angew. Chem. Int. Ed. 40 (6) (2001) 1102–1104.
[8] A.H. Janssen, A.J. Koster, K.P. de Jong, J. Phys. Chem. B 106 (2002) 11905–11909.
[9] A. Boisen, I. Schmidt, A. Carlsson, S. Dahl, M. Brorson, C.J.H. Jacobson, Chem. Commun. (2003) 958–959.
[10] P.A. Midgley, M. Weyland, J.M. Thomas, B.F.G. Johnson, Chem. Commun. (2001) 907–908.
[11] M. Weyland, P.A. Midgley, J.M. Thomas, J. Phys. Chem. B 1005 (2001) 7882–7886.
[12] U. Ziese, C. Kübel, A.J. Verkleij, A.J. Koster, J. Struct. Biol. 138 (1–2) (2002) 58–62.
[13] U. Ziese, Unpublished results, 2003.
[14] M. Weyland, P.A. Midgley, Microsc. Microanal. 7 (Suppl. 2) (2001) 1162–1163.
[15] G. Möbus, B.J. Inkson, Appl. Phys. Lett. 79 (2001) 1369–1371.
[16] W. Baumeister, R. Grimm, J. Walz, Trends Cell Biol. 9 (1999) 81–85.
[17] B.F. McEwen, M. Marko, J. Histochem. Cytochem. 49 (2001) 553–563.
[18] A.J. Koster, H. Chen, J.W. Sedat, D.A. Agard, Ultramicroscopy 46 (1992) 207–227.
[19] K. Dierksen, D. Typke, R. Hegerl, A.J. Koster, W. Baumeiester, Ultramicroscopy 40 (1992) 71–87.
[20] U. Ziese, A.H. Janssen, W.J.C. Geerts, T. Krift, A. van Balen, H. de Ruiter, K.P. de Jong, A.J. Verkleij, A.J. Koster, Microsc. Microanal. 7 (Suppl. 2) (2001) 78–79.
[21] U. Ziese, A.H. Janssen, J.L. Murk, W.J.C. Geerts, T. Krift, A.J. Verkleij, A.J. Koster, J. Microsc. 205 (2) (2002) 187–200.
[22] K.P. de Jong, A.J. Koster, Chem. Phys. Chem. 3 (2002) 776–780.
[23] P.A. Midgley, M. Weyland, Ultramicroscopy 96 (3–4) (2003) 413–431.
[24] G. Möbus, R.C. Doole, B.J. Inkson, Ultramicroscopy 96 (3–4) (2003) 433–451.

Ulrike Ziese[*]
Krijn P. de Jong
Department of Inorganic Chemistry and Catalysis
Utrecht University, Sorbonnelaan 16
3584 CA Utrecht, The Netherlands
[*]Corresponding author
E-mail address: u.ziese@chem.uu.nl (U. Ziese)

Abraham J. Koster
Department of Molecular Cell Biology
Utrecht University, Padualaan 8
3584 CH Utrecht, The Netherlands

8 October 2003